Chemical Science

ROYAL SOCIETY OF CHEMISTRY

EDGE ARTICLE

View Article Online
View Journal | View Issue

Cite this: *Chem. Sci.*, 2020, **11**, 4695

All publication charges for this article have been paid for by the Royal Society of Chemistry

Received 6th February 2020
Accepted 14th April 2020

DOI: 10.1039/d0sc00714e

rsc.li/chemical-science

Thiophene-fused polyaromatics: synthesis, columnar liquid crystal, fluorescence and electrochemical properties†

Yifan Li, Alberto Concellón, Che-Jen Lin, Nathan A. Romero, Sibo Lin and Timothy M. Swager *

Efficient syntheses that incorporate thiophene units into different extended conjugation systems are of interest as a result of the prevalence of sulfur-rich aromatics in organic electronics. Self-organization by using liquid crystal properties is also desirable for optimal processing of organic electronics and optical devices. In this article, we describe a two-step process to access extended regioisomers of polyaromatics with different shapes. This method involves an efficient single or double benzannulation from an alkyne precursor followed by Scholl cyclization. In spite of their unconventional nondiscoid shape, these materials display stable columnar liquid crystal phases. We examine the photophysical and electrochemical properties and find that structurally very similar thiophene-fused polyaromatics display significant differences in their properties.

Introduction

Extended polycyclic aromatic hydrocarbons (PAHs) with precise structures enable many organic electronic devices, including organic light emitting diodes (OLEDs), organic field-effect transistors (OFETs), and organic photovoltaic devices (OPVs).[1] Thiophene-based materials dominate organic semiconducting materials as a result of their versatile/unique chemistry and electronic properties.[2] Of particular interest is the fact that thiophene containing PAHs in ordered arrangements can offer enhanced performance in organic electronic devices.[2d,3] Liquid crystals self-organize in fluid states for superior processing into highly organized anisotropic self-healing structures.[4]

Disk-shaped molecules consisting of π-conjugated PAH rigid cores and disordered sidechains are the basis of many columnar thermotropic liquid crystals.[5] The resultant organizations provide strong intermolecular π–π stacking, resulting in one-dimensional electronic correlations and associated anisotropic charge-carrier transport. The design of new PAH cores is key to extend the electronic performance of liquid crystalline organic materials. To this end, there have been previous investigations of thiophene-containing liquid crystalline semiconductive molecules. Oligothiophene derivatives end-capped with alkyl chains display liquid crystalline properties and self-organize into lamellar (smectic) structures.[6] Discotic liquid crystals that contain thiophene-fused units are attractive candidates for organic electronics. However, the number of thiophene-containing columnar liquid crystals is limited when compared to their calamitic liquid crystals relatives.[7]

Alkynes are a widely used efficient precursor to nanographenes. Our group has a long-standing interest in accessing PAHs *via* efficient alkyne benzannulation reactions,[8] which has been expanded considerably in scope by others in recent years.[9] We report herein the design and synthesis of columnar self-assembling systems based on thiophene-fused PAHs *via* alkyne benzannulation followed by oxidative coupling reactions. All the compounds are fluorescent, and despite their non-discoid shapes, stable enantiotropic columnar liquid crystal phases are observed. The self-assembled columnar structure was studied by X-ray diffraction. Interestingly, small differences in the position and orientation of the thiophene moieties in the molecules has significant impact on their photoluminescence in solution and in the solid state and their electrochemical behaviour.

Results and discussion

Synthesis

Our initial efforts focused on the oxidative annulation of biaryl acetylene (**1a**) to directly access dithienochrysene (**3a**).[8d] Commonly used oxidative conditions such as $SbCl_5$, $FeCl_3$, $MoCl_5$ and DDQ/TFA only led to uncontrolled decomposition of starting materials. As a result, we turned our attention to a stepwise procedure, fusing one thienyl moiety per step. Several gold and platinum catalysts[10] as well as strong Brønsted acids[8a] were tested for the first benzannulation, giving desired

Department of Chemistry, Massachusetts Institute of Technology, 77 Massachusetts Ave, Cambridge, MA 02143, USA. E-mail: tswager@mit.edu

† Electronic supplementary information (ESI) available: Experimental procedures, additional information, and characterization data. See DOI: 10.1039/d0sc00714e

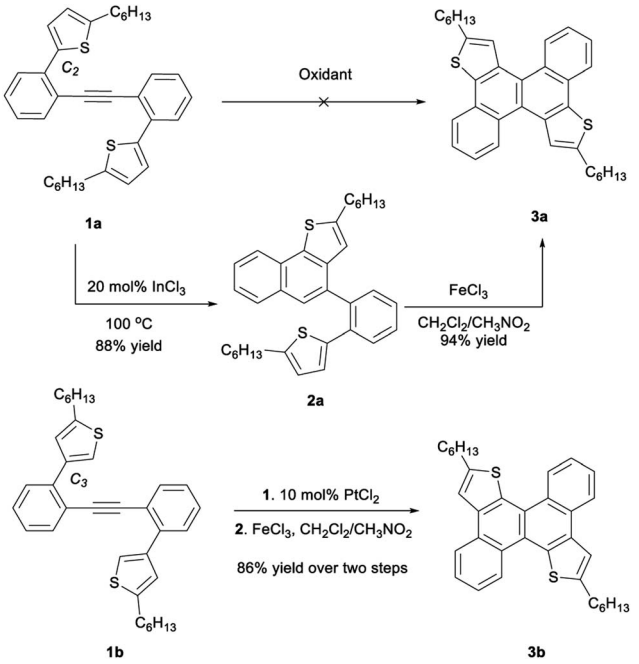

Scheme 1 Stepwise transformation of alkynes to thiophene-fused polyaromatics.

intermediate **2** in moderated yields, but these conditions also gave an inseparable unidentified impurity. However intermediate **2** is successfully produced in pure form in 88% yield by treatment with 20 mol% of $InCl_3$ in toluene at 100 °C for 12 hours.[9b] Reaction of **2** with a mixture of $FeCl_3$ in dichloromethane (DCM)/CH_3NO_2 gave dithienochrysene (**3a**) in 94% yield after 15 minutes (Scheme 1). When the thiophenes are linked *via* C_3 positions in the starting biaryl acetylene **1b**, 10 mol% $PtCl_2$ proves to be the optimal reagent for the alkyne annulation; after Scholl reaction, isomeric dithienochrysene **3b** was obtained in 86% overall yield. This high-yielding transformation allows us to access an extended, thiophene fused conjugated system.

To obtain oligomeric fused systems, we subsequently applied this two-step transformation to di-acetylene precursors with both C_2 and C_3 connectivity to the thiophenes (Scheme 2 and see the ESI† for detailed syntheses). The initial $InCl_3$-catalyzed benzannulation for di-alkynes gives a mixture of regioisomers. However, these new rings are desired connections for the same final products after the second cyclization. For the thiophene C_2 linked precursors, the yields of annulation are generally moderate using 0.2 eq. of $InCl_3$. The efficiency of this step can be significantly improved by using 0.4 eq. of catalyst.[11] For the dual benzannulation of the C_3-linked thiophene starting materials, 10 mol% of $PtCl_2$ delivered cyclized products in 67–83% yield. Submitting the isolated regioisomeric mixtures to oxidative Scholl reaction conditions affords thiophene fused polyaromatics (**4a–6a** and **4b–6b**) in good overall yield. Starting from *para*-, *meta*-, and *ortho*-substituted dialkynylbenzene cores and C_2- or C_3-attached thiophene regioisomers, we obtained rapid access to a library of thiophene-fused conjugated systems with different shapes.

Liquid crystal properties

Thermal stability is required for melt processing and was studied by thermogravimetric analysis (TGA). In most of the cases the 5% weight loss temperature ($T_{5\%}$) was detected more than 100 °C above the isotropization point (*vide infra*) (Table 1). The thermal transitions and liquid crystal properties were studied by polarizing optical microscopy (POM) and differential scanning calorimetry (DSC) as summarized in Table 1. Compounds **4a**, **4b**, **5a**, and **5b** exhibited stable enantiotropic mesophases over a wide temperature range. These mesophases were assigned as hexagonal columnar on the basis of the mosaic-like textures observed by POM (Fig. S1†).[12] Compounds

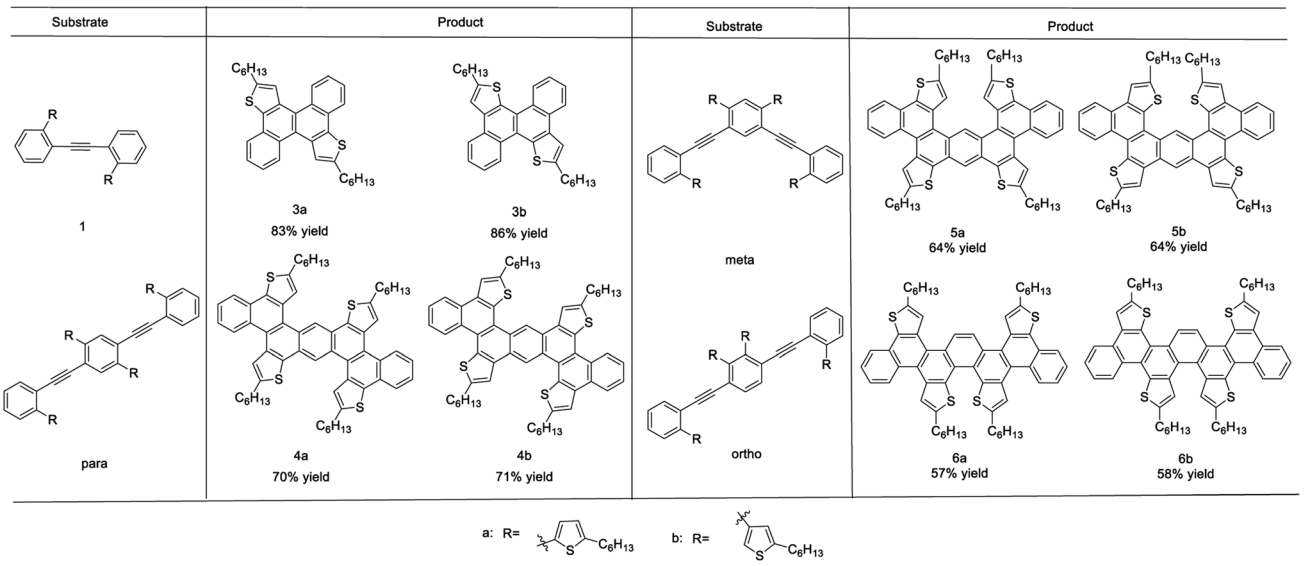

Scheme 2 Thiophene-fused conjugation system (note that overall yields are given).

Table 1 Thermal stability, liquid crystal properties, and X-ray diffraction structural parameters

	$T_{5\%}$[a] (°C)	Phase transitions[b]	Structural parameters[c]
3a	269	Cr_1 34 (5.6) Cr_2 63 (36.3) I	
3b	282	Cr 97 (47.6) I	
4a	294	Cr 72 (22.1) Col_h 140 (6.2) I	$a = 22.5$ Å; $c = 3.5$ Å
4b	236	Cr_1 110 (3.4) Cr_2 145 (26.1) 148 Col_h 215 I^{dec}	$a = 22.5$ Å; $c = 3.5$ Å
5a	389	$Col_{h(G)}$ 18 Col_h 84 (−11.8) Cr 135 (18.5) I	$a = 20.5$ Å; $c = 4.0$ Å
5b	343	$Col_{h(G)}$ 65 Col_h 194 (4.9) I	$a = 20.3$ Å; $c = 4.1$ Å
6a	398	G 75 I	
6b	426	G 202 I	

[a] Temperature at which 5% mass lost is detected in the thermogravimetric curve. [b] DSC data of the second heating process at a rate of 10 °C min^{-1}. Temperatures (°C) are read at the onset of the corresponding peaks, and enthalpies (kJ mol^{-1}) are in brackets. Cr: crystal phase, G: glass, I: isotropic liquid, Col_h: hexagonal columnar mesophase, Col_h(G): glassy hexagonal columnar mesophase, dec: decomposition. [c] Structural parameters obtained by XRD. *a*: lattice constant of the columnar phase, *c*: mean stacking distance.

4a and **4b** were crystalline materials at room temperature but exhibited liquid crystal properties at elevated temperatures. Consequently, their DSC curves showed two peaks associated to the Cr-to-Col_h and Col_h-to-I transitions (Fig. 2). In addition, the high clearing temperature at the isotropization results in some decomposition as evidenced in TGA and DSC experiments. In contrast, the DSC curves of **5a** and **5b** were reproducible through multiple thermal cycles, and cooling cycles showed only one identifiable peak corresponding to the clearing point in addition to a glass transition, which freezes the mesomorphic order at room temperature (Fig. 1). The DSC of **5a** reveals that the mesophase undergoes a cold crystallization during the second heating process. Compounds **3a** and **3b** are crystalline materials that melt to give an isotropic liquid phase without showing liquid crystalline properties. Compounds **6a** and **6b** are amorphous materials and DSC curves only show a baseline step corresponding to the glass transition. The steric interactions between thiophene–C_6H_{13} groups in **6a** and **6b** results in a twisted configuration of the aromatic core that decreases the efficiency of π–π stacking interactions that are necessary for the formation of liquid crystal mesophases (see the ESI† for detailed geometry optimization).

Although the textures observed by POM were suggestive of hexagonal columnar mesophases, the absolute assignment and the determination of the lattice parameters were achieved by X-ray diffraction (XRD). XRD experiments were carried out on samples that were cooled from the isotropic liquid. As mention before, **4b** showed some decomposition at the transition to the isotropic liquid, and thus the experiments were carried out at lower temperatures wherein the stability was confirmed by TGA and DSC experiments.

The XRD patterns of all the LC compounds contain three or four small-angle region reflections with *d*-spacings in the ratio of $1 : 1/\sqrt{3} : 1/\sqrt{4} : 1/\sqrt{7}$ arising from the (1 0 0), (1 1 0), (2 0 0), and (2 1 0) reflections of the two-dimensional hexagonal lattice in a columnar hexagonal LC arrangement (Fig. 2 and S2†). The lattice parameters (*a*) are gathered in Table 1 and we also

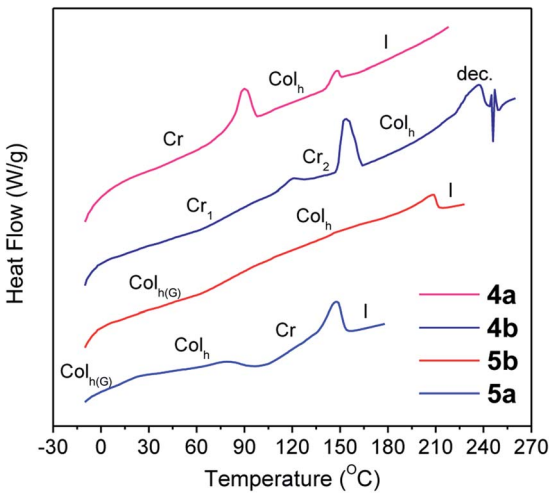

Fig. 1 DSC traces corresponding to the second heating scan (10 °C min^{-1}, exo down). (The first heating scan is shown for **4b**.)

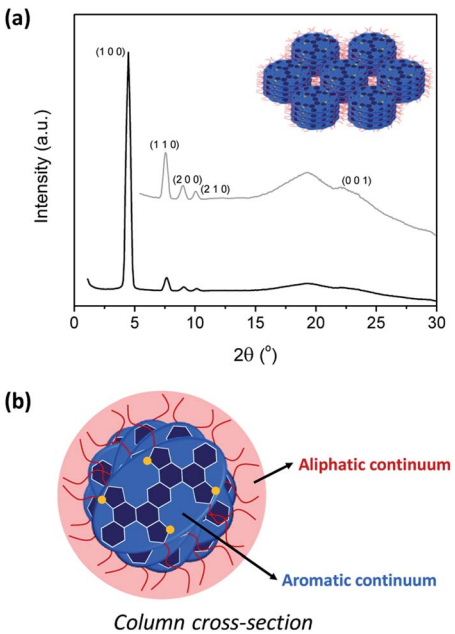

Fig. 2 (a) 1D XRD profiles of **4a**, and (b) proposed arrangement of the hexagonal columnar mesophase.

observe broad diffuse scattering in the high-angle region (d = 4.5 Å), which is characteristic of the liquid-like order of the hydrocarbon chains. Additionally, a more defined broad reflection at 3.5–4.1 Å was observed, which is indicative the periodic correlations of the cores along the columns (parameter c). The significant shortening in the π–π stacking distance (c) is found in **4a** and **4b**, when compared to **5a** and **5b**, and is consistent with our expectations. Specifically, the proximity of thiophene–C_6H_{13} units in **5a** and **5b** induces a moderate twisting of the aromatic cores, whereas **4a** and **4b** have a planar core. This feature is at the origin of the tighter packing of the units within the columns.

The hexagonal symmetry implies that columns have an average cylindrical cross-section with a uniform distribution of aliphatic chains along their periphery (aliphatic continuum). However, these LC compounds have elliptical shapes rather than the classical disk shape characteristic of many columnar liquid crystals. Therefore, these elliptic mesogens must adopt a distribution of orientations along the stacking directions and may have dynamics that likely include tilting inside and between columns to on average fill the column cross-section (Fig. 2), similar to what is observed for other non-discotic mesogens in hexagonal columnar phases.[7e,f,13] Such molecular organizations are largely driven by the nanosegregation between the aromatic cores and the aliphatic continuum, and is similar each of the mesophases examined here.

Additional support for this structural model was obtained by simple calculations based on the parameters measured by XRD. The relationship between the density (ρ) of the compounds in the mesophase and the measured XRD parameters is given by the equation $\rho = M \times Z/N_A \times V$, where M is the molar mass, Z is the number of molecules in the unit cell, N_A is Avogadro's number, and V is the unit cell volume ($V = a^2 \times \sqrt{3}/2 \times c \times 10^{-24}$). If we consider one molecule per disk ($Z = 1$), the density of the compounds was calculated to be close to 1.0 g cm^{-3} (Table S1†), which is a reasonable value for organic liquid crystalline materials. Therefore, these calculations are in good agreement with the proposed model for the packing in each column stratum of the hexagonal columnar mesophase.

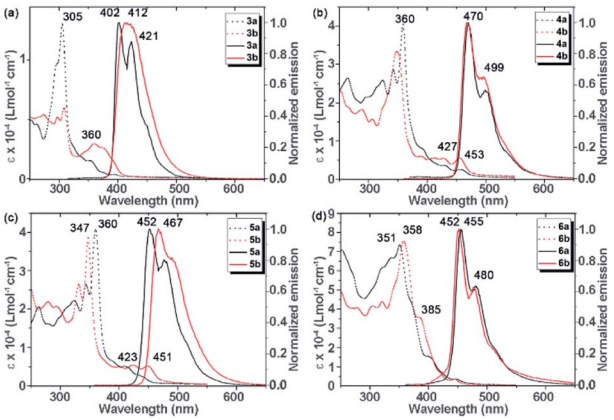

Fig. 3 Absorption spectra (dashed lines) and normalized emission spectra (solid lines) of **3a–6a** and **3b–6b** in dichloromethane.

Photophysical and electrochemical characteristics

The photophysical properties of this set of thienoacenes reveal subtle electronic variations arising from thienyl group isomerism and differential acene-backbone configurations. Thienoacenes **3a/b** exhibit strong absorptions near 300 nm, along with less intense bands on the low energy side (Fig. 3). The absorption spectra for **4a/b–6a/b** show similar transitions shifted bathochromically by roughly 60 nm, consistent with more extensive π-conjugation in **4–6** relative to **3**. While the band edges are at similar energies for **4a/b–6a/b**, the extinction coefficients (ε) for the low energy transitions are significantly larger in **3b–5b** as compared to their respective isomers **3a–5a**, but are similar to **6a** and **6b**. These characteristics are in accord with TD-DFT calculations on model structures **3a′/b′–6a′/b′**, for which calculated oscillator strengths (f) for $S_0 \rightarrow S_1$ transitions are larger in **3b′–5b′** than the corresponding isomers **3a′–5a′** and again **6a′** and **6b′** are similar in magnitude to **3b′–5b′** (see ESI† for full computational details). Solution state photoluminescence spectra reveal small Stokes shifts and relatively narrow, structured emission bands for all compounds with the exception of **3b**, which shows a broadened emission relative to **3a** (Fig. 3). While emission energies in **4a/b** and **6a/b** appear to be unaffected by thienyl substitution, the emission maximum

Table 2 Photophysical and electrochemical properties of **3a/b–6a/b**

	λ_{abs}[a] (nm)	ε (Lmol^{-1} cm^{-1})	λ_{em}[a b] (nm)	Φ_{em}[a c] (nm)	λ_{em}[d]	E_{p1} (V *vs.* Fc$^{+/0}$)[e]
3a	305	13 000	402 (421)	0.6%	412 (430) [Cr]	+0.84
4a	360	40 500	470 (499)	3.5%	522 [Cr]/528 [Col_h]	+0.49
5a	360	40 800	452 (477)	4.4%	498 [Col_h]	+0.57
6a	351	73 500	455 (480)	<0.1%	460 (489) [G]	+0.74
3b	309	6000	412	4.4%	449 [Cr]	+0.79
4b	348	33 400	467 (495)	14.8%	552 [Cr]/567 [Col_h]	+0.45
5b	347	38 600	467 (495)	9.3%	559 [Col_h]	+0.36
6b	358	75 400	452 (475)	0.2%	455 (485) [G]	+0.71

[a] Measured at 10^{-6} M. [b] Emission maxima in DCM solution (0–1 band was shown in parenthesis). [c] Emission quantum yield in DCM solution obtained from integrated sphere under air. [d] Emission maxima in thin film at different temperatures (0–1 band was shown in parenthesis and the phase is shown in brackets). [e] Lowest onset peak oxidation potentials determined by cyclic voltammetry. See Fig. 5 and ESI for details.

for **5b** exhibits a 15 nm bathochromic shift compared to **5a**. Emission quantum yields (Φ_{em}) are higher for isomers **3b–6b** than their counterparts **3a–6a**. This observation again reveals that the orientation of thienyl group affects the efficiency of radiative transition (Table 2).

Solid-state fluorescence spectra of **3a**, **3b**, **6a**, and **6b** were recorded at room temperature in their solid quenched glass phases obtained by cooling from the isotropic liquid. As was performed for XRD experiments, the emission spectra for **4a**, **4b**, **5a**, and **5b** were recorded at temperatures at wherein the molecules display hexagonal columnar mesophases. Although the emission is clearly observable, the determination of quantum yields from these samples was below the limits of detection of the integrating sphere device used in this study. (Fig. 4a). The dominant emission bands were red-shifted and broadened in the solid state relative to solution measurements (Table 2, Fig. 4 and S3†). The broad emission band combined with the significant red shift in the maxima of the solid-state emission of these films are indicative of the emission arising from the aggregated state of these molecules in the solid, liquid crystalline phase.[14] Another distinctive feature of the solid-state emission spectra is a very long and relatively unstructured tail extending to 700 nm and beyond.

The electrochemical characteristics of thienoacenes **3a–6a** and **3b–6b** were investigated by cyclic voltammetry (Fig. 5, Tables 2 and S3;† potentials referenced to $Fc^{+/0}$). All compounds undergo oxidation at relatively low potentials and exhibit no discernible reduction down to −2 V. The thienoacenes show somewhat complicated redox behaviour, with multiple overlapping oxidation events. Overall, there is a general resemblance in electrochemical behaviour on the forward (oxidative) sweep within each pair of thienoacene isomers, consistent with a previous investigation on the electrochemistry of acenedithiophenes which suggested the nature of this thienyl isomerism does not greatly impact electronic structure.[9c] The earliest onset of oxidation occurs at marginally lower potentials for compounds **3b–6b** compared to their respective isomers **3a–6a**, in correlation with DFT calculations which estimate HOMO levels in **3b′–6b′** at slightly higher energies than their counterparts **3a′–6a′** (Fig. S4†). A larger difference in redox potential was observed for compound **5b**, which is oxidized at a *ca.* 200 mV lower potential than its isomer **5a**. This correlates with a larger disparity in photophysical properties (*e.g.*, λ_{em}, Table 2) between **5a** and **5b** than for the other pairs of thienoacenes. Evidently, the electronic nature of the aromatic core in **5a**/**b** is more sensitive to heteroarene substitution pattern than the other acene structures.

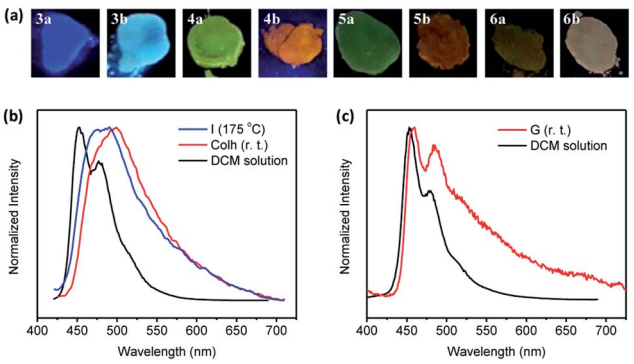

Fig. 4 (a) Pictures of the emission of the films under illumination by a 365 nm UV lamp. (b) Normalized emission spectra of **4a** in DCM and thin film at different temperatures (I: isotropic liquid, Col_h: hexagonal columnar mesophase). (c) Normalized emission spectra of **6b** in DCM and thin film at different temperatures (G: glass phase).

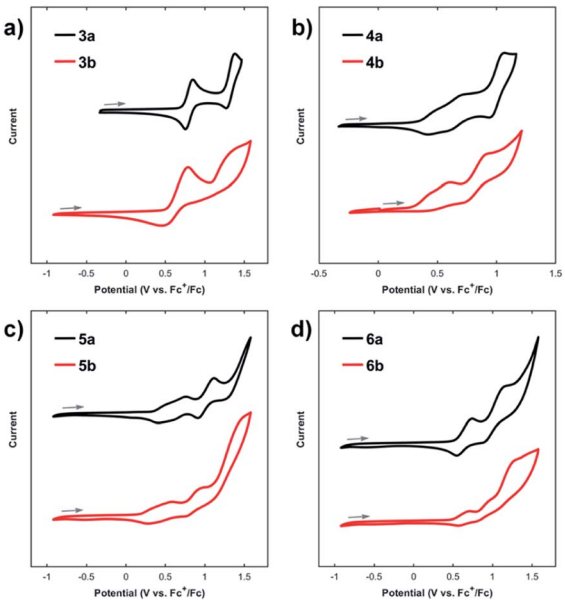

Fig. 5 Cyclic voltammograms of (a) compounds **3a** and **3b**, (b) compounds **4a** and **4b**, (c) compounds **5a** and **5b**, and (d) compounds **6a** and **6b**. Experiments were conducted at a scan rate of 100 mV s^{-1} with a glassy carbon working electrode, a platinum wire counter electrode, and an $Ag/AgNO_3$ pseudo-reference electrode. Analysis of compounds **3a–6a**, **3b** and **5b–6b** was conducted in 100 mM $[Bu_4N][PF_6]$ in DCM, and in 80 mM $[Bu_4N][PF_6]$ in *o*-DCB for **4b**. Potentials referenced to ferrocene as an external standard.

Compounds **3a–6a** display greater redox-reversibility than their respective isomers **3b–6b**, which show decreased cathodic current on the reductive sweep of the voltammogram. This behaviour is particularly evident for thienoacene **3a**, which exhibits two clear quasi-reversible oxidation events at +0.80 and +1.32 V in stark contrast to isomer **3b** (Fig. 5a). The diminished electrochemical reversibility of **3b–6b** likely arises from irreversible follow-up chemical reactions upon oxidation, which we attribute to oxidative coupling at the 3-position (*i.e.*, β-carbon) of the thienyl groups, in accord with prior literature on oxidative homocoupling of 2-substituted benzothiophenes.[15] Whereas the thienyl β-carbons in compounds **3a–6a** reside in sterically encumbered cove regions, compounds **3b–6b** all possess β-carbons located in more accessible bay regions and are likely more prone to oxidative oligomerization. These steric differences are apparent in the computed structures **3a′–6a′**/**3b′–6b′**. Thus, steric crowding in compounds **3a–6a** may enhance the kinetic stability of higher oxidation states and could account for their improved electrochemical reversibility relative to isomers **3b–6b**.

Conclusions

In conclusion, we have developed an efficient two-step process to access thiophene-fused polyaromatics from easily accessible starting materials in high overall yield. The practicality of the process is reflected by the efficient synthesis of a library of eight PAHs. These elliptical shaped molecules display hexagonal columnar liquid crystal phases. Two have low clearing temperatures and organized alignment at room temperature. All the PAHs are fluorescent at solid state. The UV-absorption and emission in solution, frontier molecular orbitals and electrochemical properties were studied, showing the role of thiophene connectivity in determining these properties. These synthetic methods have utility for the production of thiophene-fused graphene nanoribbons, and these studies are ongoing.

Conflicts of interest

The authors declare no competing financial interest.

Acknowledgements

Y. L. is grateful to the Swiss National Science Foundation (SNSF) for a postdoctoral mobility fellowship (P2ELP2_165170). C. L. thanks the Minister of Science and Technology, Taiwan, for postdoc fellowship (106-2917-I-564-058). N. A. R. acknowledges support from a National Institutes of Health postdoctoral fellowship (F32 GM126643). This research was supported the Air Force Office of Scientific Research AFOSR Grant # 17RT0904, FA9550-18-1-0341.

Notes and references

1 (*a*) J. Wu, W. Pisula and K. Müllen, *Chem. Rev.*, 2007, **107**, 718; (*b*) M. Watanabe, K.-Y. Chen, Y. Chang and T. Chow, *Acc. Chem. Res.*, 2013, **46**, 1606; (*c*) M. Ball, Y. Zhong, Y. Wu, C. Schenck, F. Ng, M. Steigerwald, S. Xiao and C. Nuckolls, *Acc. Chem. Res.*, 2015, **48**, 267; (*d*) M. Emi Cinar and T. Ozturk, *Chem. Rev.*, 2015, **115**, 3036; (*e*) T. Wöhrle, I. Wurzbach, J. Kirres, A. Kostidou, N. Kapernaum, J. Litterscheidt, J. C. Haenle, P. Staffeld, A. Baro, F. Giesselmann and S. Laschat, *Chem. Rev.*, 2016, **1116**, 1139.

2 (*a*) I. F. Perepichka and D. F. Perepichka, *Handbook of Thiophene-Based Materials,* Wiley-VCH, Weinheim, 2009; (*b*) W. Wu, Y. Liu and D. Zhu, *Chem. Soc. Rev.*, 2010, **39**, 1489; (*c*) L. Zhang, C.-A. Di, G. Yu and Y. Liu, *J. Mater. Chem.*, 2010, **20**, 7059; (*d*) H. Dong, C. Wang and W. Hu, *Chem. Commun.*, 2010, **46**, 5211; (*e*) K. Takimiya, S. Shinamura, I. Osaka and E. Miyazaki, *Adv. Mater.*, 2011, **23**, 4347.

3 (*a*) J. E. Anthony, *Chem. Rev.*, 2006, **106**, 5028; (*b*) W. Jiang, Y. Li and Z. Wang, *Chem. Soc. Rev.*, 2013, **42**, 6113.

4 (*a*) T. Kato, J. Uchida, T. Ichikawa and T. Sakamoto, *Angew. Chem., Int. Ed.*, 2018, **57**, 4355; (*b*) T. Kato, M. Yoshio, T. Ichikawa, B. Soberats, H. Ohno and M. Funahashi, *Nat. Rev. Mater.*, 2017, **2**, 17001; (*c*) A. Concellón, M. Marcos, P. Romero, J. L. Serrano, R. Termine and A. Golemme, *Angew. Chem., Int. Ed.*, 2017, **56**, 1259; (*d*) M. O'Neill and S. M. Kelly, *Adv. Mater.*, 2011, **23**, 566.

5 (*a*) W. Pisula, X. Feng and K. Müllen, *Adv. Mater.*, 2010, **22**, 3634; (*b*) B. Zhao, B. Liu, R. Q. Png, K. Zhang, K. A. Lim, J. Luo, J. Shao, P. K. H. Ho, C. Chi and J. Wu, *Chem. Mater.*, 2010, **22**, 435; (*c*) W. Yuan, X. Ren, M. Li, H. Guo, Y. Han, M. Wu, Q. Wang, M. Li and Y. Chen, *Angew. Chem., Int. Ed.*, 2018, **57**, 6161.

6 (*a*) A. J. J. M. van Breemen, P. T. Herwig, C. H. T. Chlon, J. Sweelssen, H. F. M. Schoo, S. Setayesh, W. M. Hardeman, C. A. Martin, D. M. de Leeuw, J. J. P. Valeton, C. W. M. Bastiaansen, D. J. Broer, A. R. Popa-Merticaru and S. C. J. Meskers, *J. Am. Chem. Soc.*, 2006, **128**, 2336; (*b*) K. Oikawa, H. Monobe, K. Nakayama, T. Kimoto, K. Tsuchiya, B. Heinrich, D. Guillon, Y. Shimizu and M. Yokoyama, *Adv. Mater.*, 2007, **19**, 1864; (*c*) Y. Shimizu, K. Oikawa, K. Nakayama and D. Guillon, *J. Mater. Chem.*, 2007, **17**, 4223; (*d*) F. Lincker, B. Heinrich, R. D. Bettignies, P. Rannou, J. Pécaut, B. Grévin, A. Pron, B. Donnio and R. Demadrille, *J. Mater. Chem.*, 2011, **21**, 5238; (*e*) L. Mazur, A. Castiglione, K. Ocytko, F. Kameche, R. Macabies, A. Ainsebaa, D. Kreher, B. Heinrich, B. Donnio, S. Sanaur, E. Lacaze, J. Fave, K. Matczyszyn, M. S. Jeong, W. Wu, A. Attias, J. Ribierre and F. Mathevet, *Org. Electron.*, 2014, **15**, 943; (*f*) Y. Funatsu, A. Sonoda and M. Funahashi, *J. Mater. Chem. C*, 2015, **3**, 1982; (*g*) A. Richard, V. Lemaur, Y. Olivier, J. Cornil, A. R. Kennedy, Y. Diao, W. Lee, S. Mannsfeld, Z. Bao and Y. H. Geerts, *J. Mater. Chem. C*, 2015, **3**, 674.

7 (*a*) T. Yasuda, H. Ooi, J. Morita, Y. Akama, K. Minoura, M. Funahashi, T. Shimomura and T. Kato, *Adv. Funct. Mater.*, 2009, **19**, 411; (*b*) T. Yasuda, T. Shimizu, F. Liu, G. Ungar and T. Kato, *J. Am. Chem. Soc.*, 2011, **133**, 13437; (*c*) L. Chen, S. R. Puniredd, Y. Tan, M. Baumgarten, U. Zschieschang, V. Enkelmann, W. Pisula, X. Feng, H. Klauk and K. Müllen, *J. Am. Chem. Soc.*, 2012, **134**, 17869; (*d*) Q. Xiao, T. Sakurai, T. Fukino, K. Akaike, Y. Honsho, A. Saeki, S. Seki, K. Kato, M. Takata and T. Aida, *J. Am. Chem. Soc.*, 2013, **135**, 18268; (*e*) C. Liu, H. Wang, J. Du, K. Zhao, P. Hu, B. Wang, H. Monobe, B. Heinrich and B. Donnio, *J. Mater. Chem. C*, 2018, **6**, 4471; (*f*) K.-C. Zhao, J.-Q. Du, H.-F. Wang, K.-Q. Zhao, P. Hu, B.-Q. Wang, H. Monobe, B. Heinrich and B. Donnio, *Chem.–Asian J.*, 2019, **14**, 462.

8 (*a*) M. B. Goldfinger and T. M. Swager, *J. Am. Chem. Soc.*, 1994, **116**, 7895; (*b*) M. B. Goldfinger, K. B. Crowfold and T. M. Swager, *J. Am. Chem. Soc.*, 1997, **119**, 4578; (*c*) M. B. Goldfinger, K. B. Crowfold and T. M. Swager, *J. Org. Chem.*, 1998, **63**, 1676; (*d*) S. Yamaguchi and T. M. Swager, *J. Am. Chem. Soc.*, 2001, **123**, 12087; (*e*) J. M. W. Chan, J. R. Tischler, S. E. Kooi, V. Bulovic and T. M. Swager, *J. Am. Chem. Soc.*, 2009, **131**, 5659; (*f*) T. Ikai, T. Yohida, K. Shinohara, T. Taniguchi, T. Y. Wada and T. M. Swager, *J. Am. Chem. Soc.*, 2019, **141**, 4696.

9 (*a*) S. Yamaguchi, C. Xu and K. Tamao, *J. Am. Chem. Soc.*, 2003, **125**, 13662; (*b*) V. Mamane, P. Hannen and A. Fürstner, *Chem.–Eur. J.*, 2004, **10**, 4556; (*c*) S. Shinamura,

I. Osaka, E. Miyazaki, A. Nakao, M. Yamagishi, J. Takeya and K. Takimiya, *J. Am. Chem. Soc.*, 2011, **133**, 5024; (*d*) L. Meng, T. Fujikawa, M. Kuwayama, Y. Segawa and K. Itami, *J. Am. Chem. Soc.*, 2016, **138**, 10351; (*e*) W. Yang, J. Monteiro, A. de Bettencourt-Dias, V. J Catalano and W. A. Chalifoux, *Angew. Chem., Int. Ed.*, 2016, **55**, 10427; (*f*) R. K. Mohamed, S. Mondal, J. V. Guerrera, T. M Eaton, T. E. Albrecht-Schmitt, M. Shatruk and I. V. Alabugin, *Angew. Chem., Int. Ed.*, 2016, **55**, 12054–12058; (*g*) Y. Li, G. Gryn'ova, F. Saenz, X. Jeanbourquin, K. Sivula, C. Corminboeuf and J. Waser, *Chem.–Eur. J.*, 2017, **23**, 8058; (*h*) W. Yang, G. Longhi, S. Abbate, A. Lucotti, M. Tommasini, C. Villani, V. J. Catalano, A. O. Lykhin, S. A. Varganov and W. A. Chalifoux, *J. Am. Chem. Soc.*, 2017, **139**, 13102; (*i*) H. Lin, N. Mitoma, L. Meng, Y. Segawa, A. Wakamiya and K. Itami, *Mater. Chem. Front.*, 2018, **2**, 275.

10 (*a*) A. Fürstner and P. W. Davies, *Angew. Chem., Int. Ed.*, 2007, **46**, 3410; (*b*) A. S. K. Hashmi, *Chem. Rev.*, 2007, **107**, 3180.

11 W. Yang, R. R. Kazemi, N. Karunathilake, V. J. Catalano, M. A. Alpuche-Aviles and W. A. Chalifoux, *Org. Chem. Front.*, 2018, **5**, 2288.

12 (*a*) K. Zhao, L. An, X. Zhang, W. Yu, P. Hu, B. Wang, J. Xu, Q. Zeng, H. Monobe, Y. Shimizu, B. Heinrich and B. Donnio, *Chem.–Eur. J.*, 2015, **21**, 10379; (*b*) V. Iguarbe, A. Concellón, R. Termine, A. Golemme, J. Barberá and J. L. Serrano, *ACS Macro Lett.*, 2018, **7**, 1138.

13 B. Donnio, B. Heinrich, H. Allouchi, J. Kain, S. Diele, D. Guillon and D. W. Bruce, *J. Am. Chem. Soc.*, 2004, **126**, 15258.

14 (*a*) S. Varghese, N. S. S. Kumar, A. Krishna, D. S. S. Rao, S. K. Prasad and S. Das, *Adv. Funct. Mater.*, 2009, **19**, 2064; (*b*) D. D. Prabhu, N. S. S. Kumar, A. P. Sivadas, S. Varghese and S. Das, *J. Phys. Chem. B*, 2012, **116**, 13071.

15 (*a*) T. Wirtanen, M. K. Mäkelä, J. Sarfraz, P. Ihalainen, S. Hietala, M. Melchionna and J. Helaja, *Adv. Synth. Catal.*, 2015, **357**, 3718; (*b*) L. Bering, F. m. Paulussen and A. P. Antonchick, *Org. Lett.*, 2018, **20**, 1978.